



Universiteit  
Leiden  
The Netherlands

## Phenotypic screening with 3D cell-based assays

Booij, T.H.

### Citation

Booij, T. H. (2017, December 20). *Phenotypic screening with 3D cell-based assays*. Retrieved from <https://hdl.handle.net/1887/59503>

Version: Not Applicable (or Unknown)

License: [Licence agreement concerning inclusion of doctoral thesis in the Institutional Repository of the University of Leiden](#)

Downloaded from: <https://hdl.handle.net/1887/59503>

**Note:** To cite this publication please use the final published version (if applicable).

Cover Page



Universiteit Leiden



The following handle holds various files of this Leiden University dissertation:  
<http://hdl.handle.net/1887/59503>

**Author:** Booi, T.H.

**Title:** Phenotypic screening with 3D cell-based assays

**Issue Date:** 2017-12-20

## chapter 4

# High-throughput phenotypic screening of kinase inhibitors to identify drug targets for polycystic kidney disease

Tijmen H. Booij<sup>1</sup>, Hester Bange<sup>1</sup>, Wouter N. Leonhard<sup>2</sup>,  
Kuan Yan<sup>3</sup>, Michiel Fokkelman<sup>1</sup>, Steven J. Kunnen<sup>2</sup>,  
Johannes G. Dauwerse<sup>2</sup>, Yu Qin<sup>1</sup>, Bob van de Water<sup>1</sup>,  
Gerard J.P. van Westen<sup>4</sup>, Dorien J.M. Peters<sup>2</sup>, Leo S. Price<sup>1,3</sup>

- 1 Division of Toxicology, Leiden Academic Centre for Drug Research, Leiden, The Netherlands
- 2 Human Genetics, Leiden University Medical Center, Leiden, The Netherlands
- 3 Ocello B.V., Leiden, The Netherlands
- 4 Division of Medicinal Chemistry, Leiden Academic Centre for Drug Research, Leiden, The Netherlands

Based on: Booij TH, Bange H, Leonhard WN, Yan K, Fokkelman M, Kunnen SJ, Dauwerse J, Qin Y, van de Water B, van Westen GJP, Peters DJM, Price LS: High-throughput phenotypic screening of kinase inhibitors to identify drug targets for polycystic kidney disease. *SLAS Discov*, 2017

## **Abstract**

Polycystic kidney disease (PKD) is a prevalent disorder characterized by renal cysts that lead to kidney failure. Various signaling pathways have been targeted to stop disease progression, but most interventions still focus on alleviating PKD associated symptoms. The mechanistic complexity of the disease, as well as the lack of functional *in vitro* assays for compound testing, has made drug discovery for PKD challenging.

To identify modulators of polycystic kidney disease, *Pkd1*<sup>-/-</sup> kidney tubule epithelial cells were applied to a scalable and automated 3D cyst culture model for compound screening, followed by phenotypic profiling to determine compound efficacy. We used this screening platform to screen a library of 273 kinase inhibitors to probe various signaling pathways involved in cyst growth. We show that inhibition of several targets, including aurora kinase, CDK, Chk, IGF-1R, Syk, mTOR, but, surprisingly, not PI3K, prevented forskolin-induced cyst swelling. Additionally, we show that multiparametric phenotypic classification discriminated potentially undesirable (i.e. cytotoxic) compounds from molecules inducing the desired phenotypic change, greatly facilitating hit selection and validation.

Our findings show that a pathophysiological relevant 3D cyst-culture model of PKD coupled to phenotypic profiling can be used to identify potentially therapeutic compounds and predict and validate molecular targets for PKD.

## Introduction

Polycystic kidney disease (PKD) is an inherited genetic disorder that is characterized by the formation of renal cysts that block normal tubular function and thereby cause a progressive decline in kidney function with age, typically leading to end-stage renal disease (ESRD) by the 6<sup>th</sup> decade of life. This prevalent disorder occurs in approximately 1:2500 people<sup>1</sup> and, in addition to its detrimental effects on kidney function, also affects other organs such as the liver.<sup>2</sup>

The most prevalent form of PKD, autosomal dominant polycystic kidney disease (ADPKD) is in most cases caused by mutations in the *PKD1* gene or, less commonly, in *PKD2*. *PKD1* encodes polycystin-1, which is a receptor-like protein thought to be a receptor for various WNT ligands<sup>3</sup>. *PKD2* encodes polycystin-2, which is a known ion-channel with some selectivity for calcium ions. Together polycystin-1 and polycystin-2 can function as a complex which is thought to be involved in mechanotransduction of urine flow<sup>4</sup> due to its localization in the cells' primary cilium.<sup>5</sup> The polycystin proteins also localize to other areas of the cell, including the plasma membrane<sup>4,6</sup> and the endoplasmic reticulum (ER).<sup>4</sup>

Loss-of-function mutations in either *PKD1* or *PKD2* or reduced levels of functional protein are causative for cyst formation,<sup>7</sup> but the mechanisms behind this process are still poorly understood. Dysfunction of the polycystin proteins leads to a reduction in intracellular calcium levels and a consequent rise in intracellular cyclic adenosine monophosphate (cAMP) levels due to the activation of calcium-inhibitable adenylyl cyclase 6 (AC6) and reduced activity of the calcium-dependent cAMP-dependent phosphodiesterases (PDE1/4c)<sup>8</sup>. This increase in cAMP, in turn, leads to alterations in cell proliferation, apoptosis, cell-cell and cell-matrix interactions and cell polarity.<sup>8</sup> These events are known contributors to cyst initiation and cyst growth progression.

The mechanistic complexity of this disease has made it particularly difficult to develop effective medicines. As of yet, the only EMA-approved therapy in Europe for ADPKD is Jinarc (Tolvaptan), which is a vasopressin-2 receptor antagonist, consequently requiring the patients to consume large quantities of water due to increased urine production.<sup>9</sup>

In addition to the complexity of the disease, the lack of appropriate *in vitro* assays to determine drug efficacy is a likely factor underlying the limited choice of therapies available. Traditionally, cells cultured as monolayers have been used to determine drug efficacy and toxicity, but such *in vitro* systems cannot be used to adequately recapitulate the pathophysiology of ADPKD, since cysts cannot form in a two-dimensional environment. In contrast, three-dimensional (3D) culture techniques have been developed over the past decade to address these issues and to bridge the gap between 2D monolayers and animal models. Traditionally these techniques have been generally associated with high costs and low reproducibility and scalability, but due to their physiological relevance 3D phenotypic screening techniques have become a fundamental research tool in many fields,<sup>10</sup> including cancer research.<sup>11</sup>

In order to identify effective molecules and therapeutic targets in a more physiologically relevant model, we have developed a high-content and high-throughput screening platform that uses 3D-cultured cysts and used this to screen a kinase inhibitor library with known molecular targets. This allowed us to relate compound efficacy to molecular targets potentially involved in cyst growth.

## MATERIALS AND METHODS

### *Generation and Cloning of Cell Lines*

To generate cells with reduced *Pkd1* gene expression, wild-type mouse inner medullary collecting duct (mIMCD3, ATCC® CRL-2123™) cells were transduced with a lentivirus containing a short-hairpin against *Pkd1*. Lentiviral constructs expressing shRNAs targeting *Pkd1* (TRCN0000072084, 085, 086 and 087) and a non-targeting control construct (SHC002) were obtained from the Sigma MISSION shRNA library (Sigma-Aldrich, Zwijndrecht, Netherlands). Production of lentiviruses by transfection into 293T cells has been described earlier.<sup>12</sup> Cells were selected using puromycin. Reduced *Pkd1* expression, approximately 60%, was confirmed by qPCR (supplemental figure 1A, mIMCD3 sh*Pkd1*) and cell line transduced with construct TRCN0000072084 was selected for our studies. This cell line was used for the majority of the experiments described here. In addition, *Pkd1* knockout mIMCD3 cell lines were generated (supplemental figure 2) using the dimeric CRISPR RNA-guided FokI nucleases (RFN) method<sup>13</sup> in mIMCD3 cells. In short, the RFNs for *Pkd1* exon 15 were selected using ZiFiT (<http://zifit.partners.org/ZiFiT/Disclaimer.aspx>) and cloned into vector pSQT1313neo as described previously ([http://zifit.partners.org/ZiFiT/Program\\_use.aspx#\\_CRISPR\\_RFNs](http://zifit.partners.org/ZiFiT/Program_use.aspx#_CRISPR_RFNs)) (supplemental table 1). In the pSQT1313neo construct we replaced the ampicillin gene of pSQT1313, by the kanamycin/neomycin resistance cassette of pEGFP-N1 (Clontech) in this construct, to facilitate G418 selection of clones that have taken up pSQT1313neoRFN and enrich for clones that carry a *Pkd1* exon15 deletion (pSQT1313 obtained from Addgene). One clone with the correct sequence was selected and co-transfected with pSQT1601 (Addgene) the plasmid expressing the Csy4 and dCas9-FokI fusion proteins. mIMCD3 cells were grown to 80% confluency in a 9cm petri dish and transfected with 2µg Pkd1ex15RFN and 8µg pSQT1601 DNA using Lipofectamin 2000 (Invitrogen). G418 (0.5mg/ml) selection was applied after 48 hours. After 7 days, cells were re-plated at a density of ~50 cells per 9cm plate. Single colonies were picked and analyzed using PCR with primers flanking the RFN target sites (supplemental table 2). PCR products were digested with restriction-endonuclease *PvuII*, which cuts between the Pkd1ex15RFN target sites. From clones that showed undigested PCR products, demonstrating a deletion of the *PvuII* restriction site on both alleles, the PCR products were subcloned using the TOPO® cloning kit (Invitrogen). Fifteen subclones were analyzed by Sanger sequencing. The sequences for clone 5E4 revealed a 25bp out of frame deletion on one allele and an 295bp out of frame deletion for the other allele. These cells will be denoted as mIMRFNPKD 5E4 throughout this publication.

### *Maintenance of Cell Lines*

All mIMCD<sub>3</sub> cell lines were cultured in 175-cm<sup>2</sup> culture flasks at 37°C in an environment of 5% CO<sub>2</sub> in DMEM/F12 (Ham's) culture medium (D8062, Sigma Aldrich, Zwijndrecht, Netherlands), supplemented with 10% fetal bovine serum (FBS, Gibco Fisher Scientific, Landsmeer, Netherlands), Glutamax and penicillin/streptomycin. Before maximal cell density was reached, cells were washed with 1x PBS (Sigma Aldrich, Zwijndrecht, Netherlands) and trypsinized with 1x Trypsin (Gibco Fisher Scientific, Landsmeer, Netherlands). Medium was subsequently added and cells were pelleted by centrifugation for 5 minutes at 1500rpm. The cell pellet was resuspended in FBS with 10% DMSO (Biosolve B.V., Valkenswaard, Netherlands) and frozen in aliquots to -150°C.

### *3D Cyst Assay*

For the primary screen of the SelleckChem library (Munich, Germany), cryopreserved mIMCD<sub>3</sub> cells were quick-thawed using a 37°C water bath and immediately added to Cyst-Gel (OcellO, Leiden, The Netherlands). For all subsequent experiments, including the validation screen, we modified this procedure to allow cryopreserved cells to recover in 2D culture for 72 hours prior to use in the 3D assay, which resulted in improved cyst homogeneity and overall assay performance. For all subsequent experiments therefore, cryopreserved mIMCD<sub>3</sub> cells were quick-thawed in a 37°C water bath and added to 175cm<sup>2</sup> culture flasks and cultured for 72 hours at 37°C in an environment of 5% CO<sub>2</sub> prior to initiation of the cyst assay. After 24 hours, medium was refreshed and after 72 hours the monolayer was washed with 1x PBS (Sigma Aldrich, Zwijndrecht, Netherlands) and cells were trypsinized using 1x Trypsin (Gibco Fisher Scientific, Landsmeer, Netherlands) and mixed with Cyst-Gel (OcellO, Leiden, The Netherlands). 14.5mL of cell-gel mix was pipetted to 384-well plates (Greiner mClear, Greiner Bio-One B.V., Alphen aan den Rijn, Netherlands) using a CyBi Selma 96/60 robotic liquid dispenser (Analytik Jena AG, Jena, Germany). Gel-cell mix was plated at a final cell density of 2175 cells per well. After gel polymerization at 37°C for 30 minutes, 33.5mL medium was added to each well. Cells were grown in gel for 72 hours (in order to initiate lumen formation prior to compound exposures), after which the cells were co-exposed with forskolin (Coleus Forskohlii, Calbiochem, Millipore BV, Amsterdam, Netherlands) and molecules to be tested alongside positive controls using the CyBi Selma 96/60 or a BioMek FXP (Beckman Coulter B.V., Woerden, Netherlands). After 72 hours, cultures were fixed with 4% formaldehyde (Sigma Aldrich, Zwijndrecht, Netherlands) and simultaneously permeabilized with 0.2% Triton-X100 (Sigma Aldrich, Zwijndrecht, Netherlands) and stained with 0.25mM rhodamine-phalloidin (Sigma Aldrich, Zwijndrecht, Netherlands) and 0.1% Hoechst 33258 (Sigma Aldrich, Zwijndrecht, Netherlands) in 1x PBS for 12 hours at 4°C, protected from light. After fixation and staining, plates were washed in 1x PBS for 12-24 hours, after which plates were sealed with a Greiner SilverSeal (Greiner Bio-One B.V., Alphen aan den Rijn, Netherlands) and stored at 4°C prior to imaging (screening procedure illustrated in figure 1).

### *Compounds*

A kinase inhibitor library containing 273 compounds (L1200) was obtained from

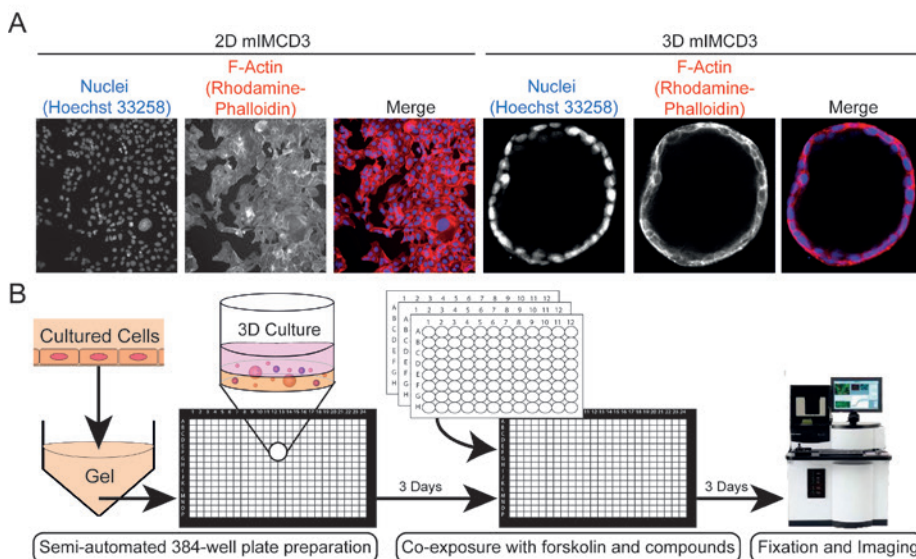


**FIGURE 1** 3D high-content screening platform that uses mIMCD<sub>3</sub> cysts grown in hydrogels as an *in vitro* model for polycystic kidney disease. **A**) mIMCD<sub>3</sub> *shPkd1* cells grown on culture plastic cannot recapitulate cystic structures (left panel); in contrast, mIMCD<sub>3</sub> *shPkd1* cells can form cysts when grown in a 3D microenvironment (right panel). **B**) 3D high-content screening platform that uses mIMCD<sub>3</sub> *shPkd1* or mIMRFNPKD 5E<sub>4</sub> cysts to determine compound efficacy.

SelleckChem (Munich, Germany), with compounds pre-dissolved to 10mM in DMSO. Analytical grade DMSO was obtained from Biosolve B.V. (Valkenswaard, Netherlands). Rapamycin, roscovitine, sorafenib tosylate, torin 1 and buparlisib (NVP-BKM-120) were purchased from SelleckChem (Munich, Germany) through distributor Bio-Connect B.V. (Huissen, Netherlands). Metformin HCl was obtained from Sigma Aldrich (Zwijndrecht, Netherlands).

### Fluorescence Microscopy

Hoechst 33258 and rhodamine-phalloidin – stained cysts in 384-well plates were imaged using a BD Pathway 855 (BD Biosciences, Breda, Netherlands) automated inverted wide-field microscope using a 4x Olympus objective. Images were obtained using BD Attovision software (BD Biosciences, Breda, Netherlands) accompanying the microscope, which was used to image focal planes throughout the gel at intervals of 50µm. The gel was imaged through its entire depth (z-axis), requiring around 25 images per well; each image captured approximately 75% of the well area (supplemental figure 3A). High-resolution confocal images were made using a 20x objective on a Nikon Ti Eclipse confocal laser microscope (lasers 561 and 408nm). Confocal images were exported using NIS Elements Viewer (Nikon Instruments Europe B.V., Amsterdam, Netherlands).

### *Image – and Data Analysis*

Images obtained with the BD Pathway 855 imager were processed through Ominer software (Ocello B.V., Leiden, Netherlands) integrated in KNIME Analytics Platform (Konstanz, Germany, <http://www.knime.org/>). This software allowed the quantification of images derived from both rhodamine-phalloidin (F-actin) and Hoechst 33258 (nuclei) image channels. This procedure is schematically represented in supplemental figure 3B. For the rhodamine-phalloidin image channel, a monochrome mask was generated for all of the individual images taken along the z-axis of the gel to define regions of interest (ROIs). This approach allowed us to quantify individual cysts – even those vertically overlapping that would otherwise have been detected as one object. These monochrome masks were used to derive shape- and size- related phenotypic descriptors of each cyst. Cyst size was derived from these monochrome masks as an area measurement of the number of pixels occupied per cyst (with approximately 100-150 cysts in each well, supplemental figure 4). The actin-dense region at the boundary of all cysts was quantified separately, so that the thickness- and shape of the cyst wall could be related to the total cyst size. Finally, to derive staining intensity-related quantifications, a maximum intensity projection of the original image stack was generated. For the Hoechst 33258 image channel, the spatial resolution upon imaging with the BD Pathway 855 was not high enough to accurately measure the shape of individual nuclei. Therefore, nuclei image stacks were immediately processed to a maximum intensity projection and processed as described earlier.<sup>14-15</sup> All phenotypic descriptors were subsequently z-score normalized to plate medians and thereafter z-scored to unstimulated control median or scaled to percent inhibition (unstimulated control median to 100%, forskolin-stimulated control median to 0%) using KNIME. For multiparametric phenotypic analysis, phenotypic descriptors were ranked based on Z-prime values  $>1.0$  between stimulated (2.5 $\mu$ M forskolin) and 10nM rapamycin-treated, forskolin-exposed control conditions for all cysts. Supplemental table 3 provides an overview of included phenotypic features. Selected phenotypic features were used for principal components analysis to condense phenotypic information to three principal components (PC<sub>0</sub>, PC<sub>1</sub> and PC<sub>2</sub>), together comprising 84% of the variation in the dataset. Principal components were exported from KNIME and visualized as a 3D scatterplot generated using the Scatterplot3D package (<https://CRAN.R-project.org/package=scatterplot3d>) for Rstudio 0.99.878 (<https://www.rstudio.com/products/rstudio2>) with R3.2.3 (<https://www.r-project.org/>). Other charts were made using the ggplot2 (<http://ggplot2.org>) package for R-Studio 0.99.878 with R3.2.3 or with Graphpad Prism 7 (Graphpad Software, La Jolla, California, USA).

### *Assessment of Synergy*

The Bliss-independence model<sup>16</sup> was used to assess potential synergistic effects. This model assumes that the effects of a certain drug are independent of those of the other drug. To apply this method, inhibition of cyst growth was scaled between 0 (no inhibition) and 1 (maximum effect). The model is given in the formula  $E = E_A + E_B - E_A E_B$ , where  $E$  is the predicted combined compound response based on the individual effect

of two compounds ( $E_A$  -torin 1 and  $E_B$  -buparlisib). This method compares the observed combination response with the predicted combined compound response  $E$  into a combination index ( $CI=(E_A+E_B-E_{AB})/E_{AB}$ ). The combination is declared synergistic if the observed effect is larger than the predicted combined response, or antagonistic if the observed response is smaller than the predicted response.

### Statistical Calculations

Unless otherwise stated in figure legends, figures represent mean and standard deviations (SD). All statistical calculations were performed in Graphpad Prism 7. Z'-factor calculations were performed after correction for number of replicates to reflect assay robustness:<sup>17</sup>

$$Z' \text{ factor} = \frac{\left( \text{AVG}_{\text{max}} - \frac{3\text{SD}_{\text{max}}}{\sqrt{n}} \right) - \left( \text{AVG}_{\text{min}} + \frac{3\text{SD}_{\text{min}}}{\sqrt{n}} \right)}{\text{AVG}_{\text{max}} - \text{AVG}_{\text{min}}} \quad \text{(EQUATION 1)}^{17}$$

In equation 1, AVG is mean and SD standard deviation of stimulated (max) or unstimulated (min) control groups, and n is the number of technical replicates.

## RESULTS

### *mIMCD3 cells form cysts in 3D hydrogels and addition of forskolin induced cyst swelling*

To identify modulators of cyst growth, we developed an automation-compatible 3D cyst growth assay, in which cyst swelling is driven by forskolin over a period of 72 hours. mIMCD3 cells with a short hairpin-mediated knockdown of *Pkd1* were cultured in extracellular matrix-based hydrogels in 384-well plates and formed cystic structures by day 3, whereas cysts could not form in 2D monolayer cultures (figure 1A). Cysts were exposed to solvent (0.2% DMSO, unstimulated) in culture medium or 2.5mM forskolin (stimulated) and responded to exposure to forskolin by increased cyst swelling (figure 1B and 2A). Cyst size was measured by quantifying object area from all individual cysts. Mean cyst area and standard deviation of 8 replicates is shown as a function of forskolin concentration and presented as z-score relative to unstimulated control median (figure 2B). It should be noted that this forskolin-driven cyst growth is an intrinsic characteristic of mIMCD3 cells, and is not dependent on the presence of polycystin-1 (supplemental figure 1B-C). Co-exposure with forskolin and rapamycin (inhibitor of mammalian target of rapamycin, mTOR), roscovitine (inhibitor of cyclin-dependent kinases; Cdc2, CDK2, CDK5<sup>18</sup>), NVP-BEZ-235 (a dual inhibitor of mTOR/PI3K<sup>19</sup> that potentially also inhibits ATM and ATR at high concentrations<sup>20</sup>) or sorafenib (sorafenib tosylate, a multikinase inhibitor targeting B-Raf and Raf-1<sup>21</sup>) prevented the increase of cyst swelling induced by forskolin (figure 2C and 2D). The increase in cyst growth by forskolin and consequent blockade of this increase by control compounds was also observed in *Pkd1* knock-out cells (mIMRFNPKD 5E4), as illustrated by three independent experiments presented in supplemental figure 5.

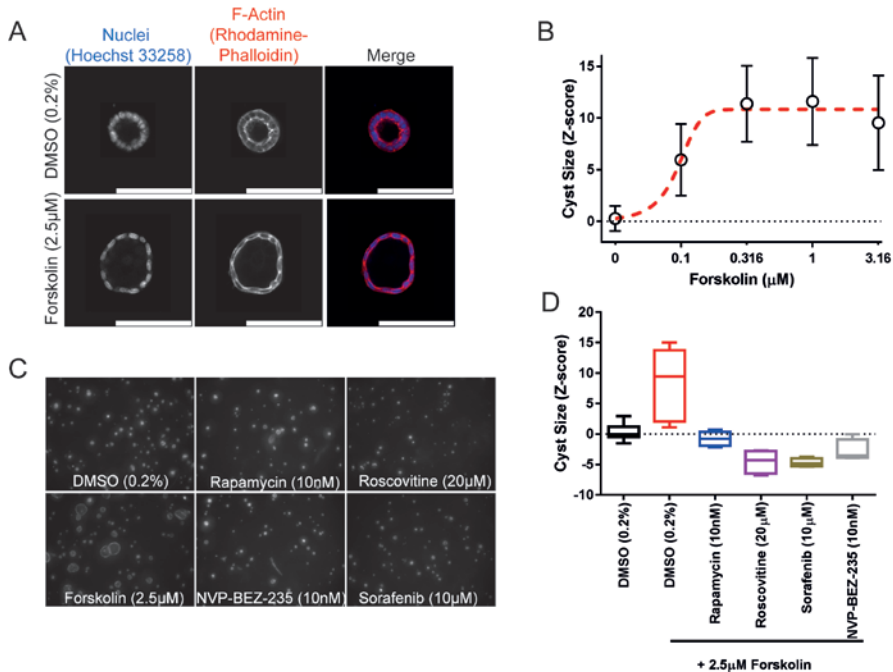


**FIGURE 2** mIMCD3 *shPkd1* cyst growth can be enhanced with forskolin and this increase can be prevented with positive control compounds rapamycin, sorafenib, roscovitine and NVP-BEZ-235. **A**) high-resolution images obtained from an unexposed (DMSO 0.2%, top panel) and a forskolin-treated (bottom panel) cyst. **B**) Using Ominer analysis tools, cyst size could be expressed as a function of forskolin concentration. Data points represent means  $\pm$ SD of 8 replicate wells (technical replicates). **C**) Representative images of control compounds after co-exposure with forskolin, including unstimulated (DMSO 0.2%) control. **D**) Quantification of average cyst size from C. Whiskers represent min to max. Rapamycin, roscovitine, sorafenib and NVP-BEZ-235 tested in quadruplicate (technical replicates), unstimulated (n=16 replicate wells) and stimulated (n=8 replicate wells). These experiments have been performed independently more than three times (supplemental figures 1B-C and 5A-C also show the performance of control molecules in biological replicates).

### Identification of modulators of cyst growth

Having established that inhibitors targeting pathways known to be important in cyst growth can also prevent cyst swelling in our model, we screened a library of 273 kinase inhibitors (SelleckChem-L1200) with described molecular targets. Therefore, in addition to potentially providing therapeutically interesting molecules, the selected hits could also be used to relate compound efficacy to the cellular signaling pathways that may be involved. mIMCD3 *shPkd1* cells were cultured in 3D hydrogels in 384-well plates in which they formed cysts over a period of 72 hours. Subsequently, we co-exposed cysts with 2.5mM forskolin and kinase inhibitors from the SelleckChem compound

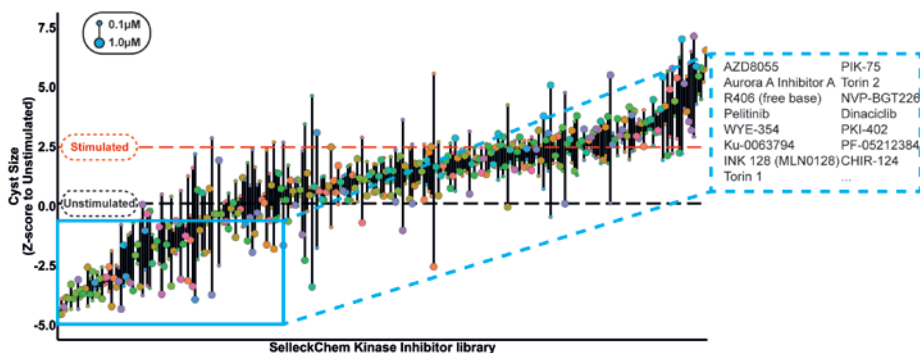


**FIGURE 3** SelleckChem kinase inhibitor library screen. Kinase inhibitors were screened in quadruplicate (technical replicates) at  $1\mu\text{M}$  and  $0.1\mu\text{M}$ , in the presence of  $2.5\mu\text{M}$  forskolin to stimulate cyst growth (procedure shown in figure 1). Data were z-score normalized to the plate median and subsequently to the unstimulated control median (unstimulated control, black striped line). Cyst growth induction by forskolin is presented by a red striped line. Compound effects are represented by means of quadruplicate wells of two tested concentrations. Top 15 hit molecules presented in right cutout. The replicate-adjusted Z'-factor for this primary screen reached  $-0.93$  between stimulated- and unstimulated control conditions.

library in quadruplicate wells at  $0.1$  and  $1\text{mM}$  for 72 hours, as illustrated in figure 1B. Cysts were then fixed and stained and imaged using the BD pathway 855 imager. Image data was processed and quantified with Ominer software and cyst size was z-score normalized to the unstimulated control median. Screening results are presented in figure 3. Forskolin induced cyst swelling and various kinase inhibitors inhibited this effect at  $0.1$  and/or  $1\text{mM}$  (figure 3). In this initial screen, we calculated an average Z'-factor of  $-0.93$  between unstimulated and stimulated controls. This weak Z'-factor appeared to be largely due to high variation between technical replicates within the stimulated control group, associated with a variable proportion of poorly expanding cysts in each well. We attributed this to sub-optimal cell health as a result of the use of cryopreserved cells in the assay, since introducing a 3-day recovery period after thawing of cryopreserved cells, improved the Z'-factor to  $+0.36$  in the validation screen. In the primary screen, active molecules were selected based on a reduction of cyst size relative to the stimulated control (red striped line) to a z-score for cyst size  $\leq 0$  (equal to or smaller than unstimulated control median) at either  $0.1$  or  $1\mu\text{M}$ . Inhibitors selected using this threshold included many inhibitors targeting mTOR, Aurora A Kinase, CDK, IGF-1R, and dual mTOR/PI3K inhibitors. For identified active molecules we obtained their respective molecular target and we validated the efficacy only of compounds with the highest affinity for these targets (shown in supplemental table 4), at six concentrations, decreasing from  $1$  or  $0.1\text{mM}$  (depending on the efficacy of the molecule in the primary screen) (figure 4A). For visualization of compound effects as a function of dose, mean cyst size of quadruplicate wells was scaled to percent inhibition of forskolin-induced cyst swell-

ing and this inhibition was presented graphically as a heat map from yellow (no inhibition) to dark blue (potent inhibition) (figure 4A). Our validation screen showed that the activity of most of the active compounds identified in the primary compound screen could be confirmed. Statistical significance was calculated using one-way ANOVA and correlated with statistical significance of the primary screen. Statistical significance was found to overlap for 58% of selected molecules (supplemental table 5). Dose-response curves for several of the compounds presented in figure 4A have been included in supplemental figure 6A-H to illustrate variation in efficacy between technical replicates. Multiparametric phenotypic analysis using principal components revealed that different compounds with different molecular targets induced novel phenotypes (figure 4B). Forskolin (empty circles) induced a phenotypic change characterized by an increase in cyst swelling, which, after principal components analysis revealed a shift in PC<sub>0</sub> and PC<sub>2</sub>. Co-exposure with either rapamycin (green) or metformin (blue) induced a phenotype indistinguishable from unstimulated controls (black). In contrast, exposure of forskolin-stimulated cysts to CDK inhibitor roscovitine (red) or B-Raf/Raf-1 inhibitor sorafenib (orange) caused this phenotypic change to overshoot, causing a novel phenotype (figures 4B, 4D). We further observed that, while roscovitine and sorafenib inhibited cyst growth similarly to rapamycin and metformin, they also appeared to have an effect on nuclei counts (supplemental figure 7), which potentially is an indication of growth inhibition or cytotoxicity related to the concentration of these inhibitors and/or due to their mechanism of action. Using this same projection model that identified the novel phenotypes of roscovitine and sorafenib, we plotted compounds targeting different kinases in the same chart (figure 4C). Indeed, other CDK inhibitors (green) such as dinaciclib were found to cluster in the same region of the PCA plot with roscovitine (figure 4B and 4C compared). In addition to the phenotype induced by dinaciclib, DNA-PK inhibitor PIK-75 (red) also induced a novel phenotype characterized by low cell count (figure 4C and 4D). Although this inhibitor would classify as a potent inhibitor of cyst growth based on cyst size (figure 4A), this molecule induced a phenotypic change that was very different to that of the unstimulated control (black). The novel phenotypes induced by dinaciclib and PIK-75 may be potentially undesirable and appear to be characterized by lower number of viable cells as shown in figure 4D.

#### *mTOR inhibitors, but not PI3K inhibitors, block forskolin-induced cyst swelling*

Based on our kinase inhibitor screen described in figure 3, we discovered that almost all mTOR inhibitors showed inhibitory activity on cyst growth, but most PI3K inhibitors showed at most only mild inhibition, which was unexpected in view of the expected role of PI3K in PKD<sup>22-24</sup>. This was confirmed using PCA based visualization and showed that mTOR inhibitors blocked the forskolin-induced phenotype, whereas PI3K inhibitors had no effect (figure 5A). We therefore re-tested a collection of 40 inhibitors that were annotated as mTOR and PI3K inhibitors from the SelleckChem library, and also tested a panel of 7 dual PI3K/mTOR inhibitors at concentrations up to 0.1 μM (figure 5B-D). Cyst size was measured and scaled to percent inhibition, denoted by a color scale from yellow (inactive) to dark blue (potent inhibition). Most mTOR inhibitors, and most notably torin 1 and -2, showed potent inhibitory activity (figure 5B), whereas most PI3K

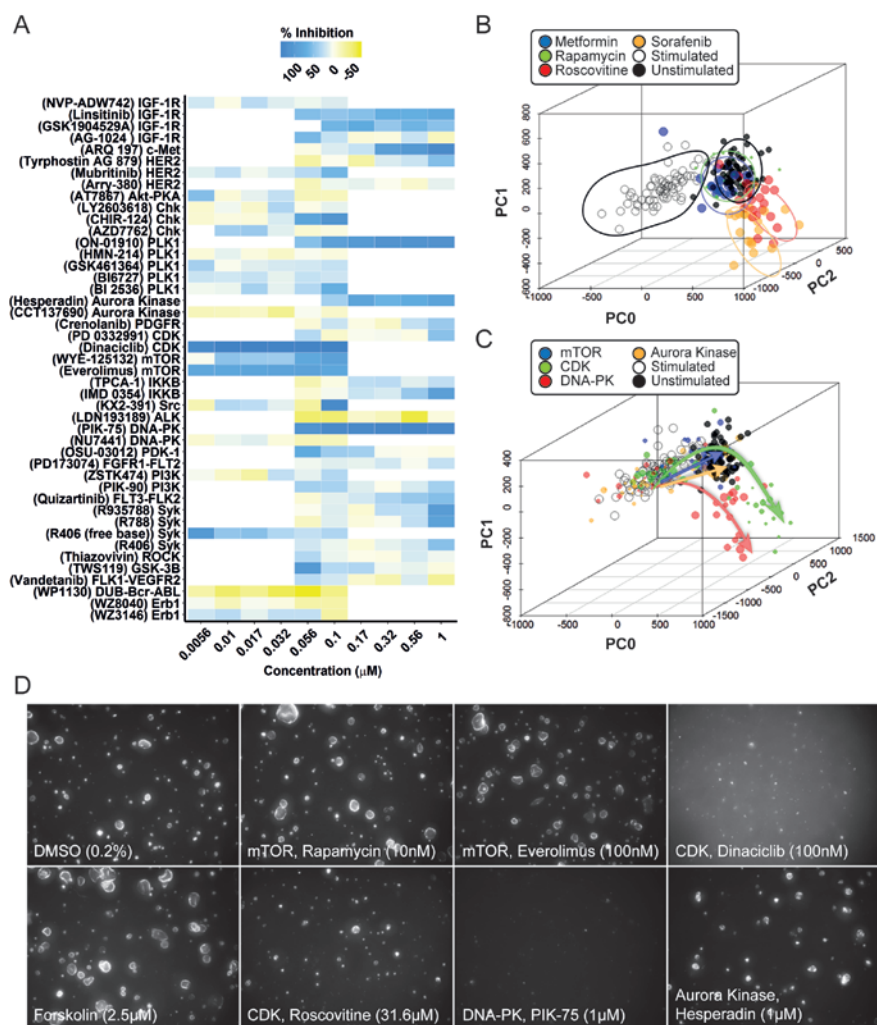


**FIGURE 4** Phenotypic analysis discriminates potentially undesirable compound effects. **A**) Validation of compounds from each target identified in figure 3. Mean percent inhibition (technical replicates representing triplicate wells) of cyst growth is depicted by a color scale from yellow (no inhibition of forskolin-induced cyst growth) to blue (complete inhibition of forskolin-induced cyst growth). Standard deviations are not included in this plot; for reference purposes several dose curves are included in supplemental figure 6. A mean  $Z^2$ -factor of +0.36 between stimulated- and unstimulated control conditions was calculated over 6 plates. **B, C**) Multiparametric (PCA) analysis (PCA plot summarizes 84% of variation in the entire dataset) identifies different compound clusters as shown by the contour plots. Forskolin-stimulated controls (large cysts) represented as empty circles, unstimulated controls (small cysts) represented as black dots. Data points represent single wells. **C**) PCA plot summarizing 84% of variation in the entire dataset. Trajectories of different compound (legend continues on next page)

types are indicated by arrows (mTOR inhibitors – blue, CDK inhibitors – green, DNA-PK inhibitors – red, aurora kinase inhibitors – orange). Data points represent single wells, point size correlates with molecule concentration (legend omitted for presentation purposes). **D**) Representative images from conditions shown as in A-C. Novel phenotypes identified in figure B and C are illustrated by images of 100nM dinaciclib and 1 $\mu$ M PIK-75.

inhibitors had low efficacy (figure 5C). We noted that the very few PI3K inhibitors that were effective at inhibiting cyst growth, may also have activity against mTOR (e.g. NVP-BGT226<sup>25</sup>). Most of the dual PI3K/mTOR inhibitors tested, showed potent inhibition of forskolin-induced cyst growth (figure 5D). We therefore considered whether PI3K, which is aberrantly active in PKD,<sup>22-23</sup> was not involved in cyst growth in our model, or whether the PI3K inhibition could exert synergistic effects together with mTOR inhibitors. To test this, we selected one mTOR inhibitor, torin 1<sup>26</sup> that displayed potent activity in our previous screens and has a 1000-fold selectivity for mTOR over PI3K<sup>27</sup> (supplemental table 4). Similarly, we selected a PI3K inhibitor, NVP-BKM120 (buparlisib), with reduced potency against mTOR<sup>28</sup> (supplemental table 4). Figure 5E shows that while both molecules show inhibition of cyst growth at high concentrations, torin 1 is a potent inhibitor at its IC<sub>50</sub> concentration, whereas buparlisib shows little activity, except at higher concentrations when it may also inhibit mTOR signaling.<sup>29</sup> Furthermore, when combined, these mTOR and PI3K inhibitors did not cause synergistic potentiation of cyst growth inhibition, as illustrated in figure 5E and supplemental figure 8, upon comparison with the predicted combined response. Based on the performed separate experiments with buparlisib and torin 1, an expected additive effect could be derived (supplemental figure 8B). Subsequently, the observed combined effect under combined exposure (e.g. 0.00316 $\mu$ M torin 1 and 0.1 $\mu$ M buparlisib) was less than this predicted effect (supplemental figure 8C). This discrepancy is reflected by a combination index (*C*) $>1$  (supplemental figure 8D). Together, these findings indicate that mTOR, but not PI3K plays a role in driving forskolin-induced cyst swelling in this model.

## Discussion

To evaluate potential targets and therapeutic modulators of polycystic kidney disease, we developed a fully-scalable high-content screening platform that uses 3D cultured cysts to quantify the effects of compounds on cyst growth. We applied this model to screen a kinase inhibitor library (SelleckChem L1200) with pre-described targets. While many small molecule kinase inhibitors often do not have one single molecular target, but rather target a range of kinases, we used this information to investigate the importance of several signaling cascades in our assay. For example, we identified many mTOR inhibitors amongst the most active compounds. The importance of mTOR in PKD has been extensively described,<sup>30-31</sup> so identification of mTOR inhibitors in our selected hits was therefore unsurprising, but confirmative of the validity of the screen. Additionally, we also identified several molecules that targeted CDK, Chk and Aurora A kinase. Since these molecules all target kinases that are important in cell cycle

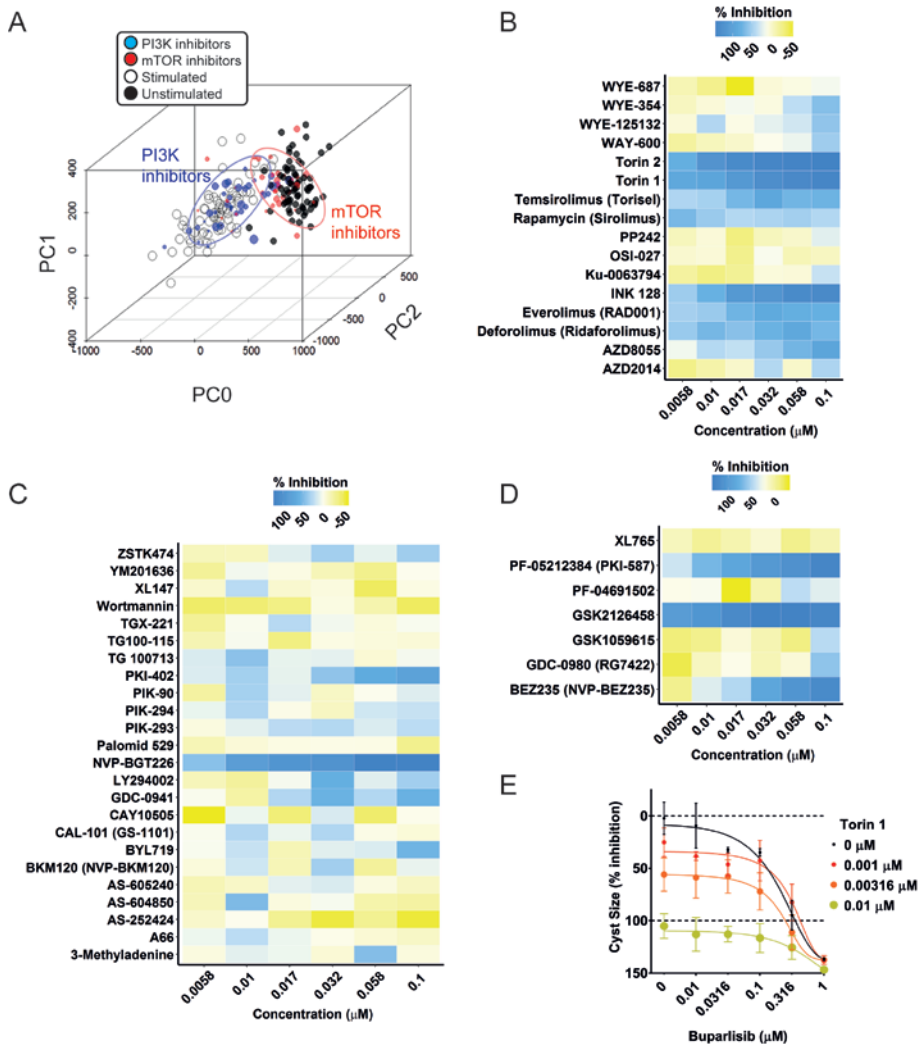


**FIGURE 5** mTOR inhibitors but not PI3K inhibitors prevent forskolin-induced cyst swelling. **A)** PCA plot comprising 84% of variation in the entire dataset. mTOR inhibitors (red circles) cluster together with unstimulated control (black dots) whereas PI3K inhibitors (blue circles) cluster with the stimulated condition (empty circles). Data points represent single wells, inhibitor point size correlates with molecule concentration (legend omitted for presentation purposes). **B)** Validation of mTOR inhibitors at concentrations 6nM to 100nM. Cyst growth inhibition displayed by a color gradient ranging from yellow (no inhibition) to blue (inhibition). The color represents the mean value of triplicate wells (technical replicates; mean Z'-factor over 8 plates of 0.28 between stimulated- and unstimulated control conditions, also for figures C and D). **C)** Validation of PI3K inhibitors; color scale as in B. **D)** Validation of dual (legend continues on next page)

PI3K/mTOR inhibitors; color scale as in B. **E)** Combination of mTOR inhibitor torin 1 with PI3K inhibitor buparlisib (NVP-BKM120) to assess synergy, in mIMRFPKD 5E4 cells. Values represent mean  $\pm$ SD of quadruplicate wells (technical replicates; Z'-factor of +0.64 between stimulated- and unstimulated control conditions)

progression, it is possible that these molecules block forskolin-induced cyst swelling by limiting proliferation or other growth-limiting effects that are potentially undesirable from a treatment perspective. Indeed, phenotypic analysis showed that especially CDK (e.g. CDK 1, -2, -5 and -9 inhibitor dinaciclib) and DNA-PK (e.g. DNA-PK and PI3K inhibitor PIK-75) inhibitors induced a novel phenotypic change, characterized by cyst sizes smaller than unstimulated control cysts and loss of cyst integrity, that could indicate a toxic effect, rather than only affecting the size of the cysts. Due to the function of CDKs in regulating the cell cycle and the function of DNA-PK in DNA-damage repair,<sup>32</sup> the identification of these growth-inhibitory effects is unsurprising. Hence, these molecules are probably not desirable for prolonged therapeutic use in asymptomatic patients.

Consistent with previous reports,<sup>33</sup> we identified several inhibitors for IGF-1R with potent inhibitory effects on cyst swelling. Some of these are also reported to have activity against the insulin receptor at the concentrations that we used, such as linsitinib, which inhibits IGF-1R with an IC<sub>50</sub> of 35nM<sup>34</sup> and the insulin receptor (IR) at 75nM. Additional studies, for example using function-blocking antibodies, are required to determine whether combined action on IGR-1R and IR are responsible for the observed effect, rather than sole inhibition of IGF-1R.

The c-Met inhibitor ArQ-197 also showed potent inhibitory activity in our assay, although other c-Met inhibitors, such as PHA-665752 and SGX-523 were inactive in the assay. This suggests that ArQ-197 may induce growth inhibitory effects independently of its effects on the c-Met receptor tyrosine kinase, which is consistent with our previous observations.<sup>15</sup> Our observation that cyst growth was reduced by IKK- $\alpha/\beta$  inhibitors suggests an involvement of the NF $\kappa$ B pathway, as previously described.<sup>35</sup> Additionally, our results hint at the involvement of spleen tyrosine kinase (Syk), which, to our knowledge, has not previously been linked to PKD. Syk may represent an interesting target for various renal diseases.<sup>36</sup> However, R788 (fostamatinib) and its active metabolite R406 may also inhibit fms-like tyrosine kinase 3 (Flt3) at the tested concentrations, so their inhibitory activity may not be solely due to inhibition of Syk (supplemental table 4, also quizartinib, an inhibitor of Flt3 displays inhibitory activity as shown in figure 4A). Interestingly, EGFR (epidermal growth factor receptor, ErbB-1) has previously been described for its involvement in cyst growth<sup>37</sup>, however, inhibitors for EGFR were not identified as hits in our screen. This may be due to the absence of added EGFR-ligands in the 3D cyst cultures. Interestingly, our screen did identify several HER2 (ErbB-2) inhibitors that reduced cyst swelling. HER2 was identified as a potential target in PKD over 10 years ago, but has received little attention since.<sup>38</sup>

Many mTOR inhibitors were selected as hits but, to our surprise, PI3K inhibitors were not, even though this has been described as a pathway involved in cyst growth.<sup>23-24</sup> We therefore tested a larger panel of inhibitors for both protein targets and found that indeed, while mTOR inhibitors showed potent efficacy, PI3K inhibitors generally lacked inhibitory activity. We also showed a lack of synergy between PI3K and mTOR inhibitors buparlisib and torin 1, indicating that PI3K does not play a role in cyst growth in this *in vitro* assay for cyst growth. However, our results do not exclude a role for PI3K in PKD patients, where cyst growth is driven by mutations in the *PKD1* or *PKD2* gene. For instance, PI3K could play a role in different phases of the disease. Furthermore, PI3K may play a more important role in the *PKHD1*-mediated recessive form of PKD.<sup>22</sup>

In conclusion, we have developed a high throughput-compatible 3D cell culture-based screening platform to identify molecules that affect cystogenesis. We have used this platform to identify molecular targets involved in cyst swelling and have identified several known- and novel pathways to be involved in cyst growth in our model. Additionally, we used multiparametric analysis to discriminate compounds that effectively inhibited cyst growth from compounds that inhibited through potentially toxic effects.

### **Declaration of Conflicting Interests**

The authors declared the following potential conflicts of interest with respect to the research, authorship, and/or publication of this article: L. S. Price is a founder and major shareholder of Ocello B.V. The other authors declared no potential conflicts of interest with respect to the research, authorship, and/or publication of this article.

### **Funding**

The authors disclosed receipt of the following financial support for the research, authorship, and/or publication of this article: T. H. Booi, W. N. Leonhard, and Y. Qin were supported by the Dutch Technology Foundation STW (Project 11823), which is part of the Netherlands Organization for Scientific Research (NWO). S. J. Kunnen was supported by NWO, Earth and Life Sciences grant 820.02.016. M. Fokkelman was supported by the EU-FP7—Systems Microscopy NoE (grant no. 258068 to B. van de Water). The other authors received no financial support for the research, authorship, and/or publication of this article.

### **References**

1. Willey CJ, Blais JD, Hall AK, Krasa HB, Makin AJ, Czerwiec FS: Prevalence of autosomal dominant polycystic kidney disease in the European Union. *Nephrol Dial Transplant*, 2016
2. Torres VE, Harris PC, Pirson Y: Autosomal dominant polycystic kidney disease. *Lancet* 369(9569): 1287-1301, 2007
3. Kim S, Nie H, Nesin V, Tran U, Outeda P, Bai CX, Keeling J, Maskey D, Watnick T, Wessely O, Tsiokas L: The polycystin complex mediates Wnt/Ca(2+) signalling. *Nat Cell Biol* 18(7): 752-764, 2016

4. Retailliau K, Duprat F: Polycystins and partners: proposed role in mechanosensitivity. *J Physiol* 592(12): 2453-2471, 2014
5. Kotsis F, Boehlke C, Kuehn EW: The ciliary flow sensor and polycystic kidney disease. *Nephrol Dial Transplant* 28(3): 518-526, 2013
6. Ibraghimov-Beskrovnaya O, Dackowski WR, Foggensteiner L, Coleman N, Thiru S, Petry LR, Burn TC, Connors TD, Van Raay T, Bradley J, Qian F, Onuchic LF, Watnick TJ, Piontek K, Hakim RM, Landes GM, Germino GG, Sandford R, Klinger KW: Polycystin: in vitro synthesis, in vivo tissue expression, and subcellular localization identifies a large membrane-associated protein. *Proc Natl Acad Sci U S A* 94(12): 6397-6402, 1997
7. Ong AC, Harris PC: A polycystin-centric view of cyst formation and disease: the polycystins revisited. *Kidney Int* 88(4): 699-710, 2015
8. Torres VE, Harris PC: Strategies targeting cAMP signaling in the treatment of polycystic kidney disease. *J Am Soc Nephrol* 25(1): 18-32, 2014
9. Blair HA, Keating GM: Tolvaptan: A Review in Autosomal Dominant Polycystic Kidney Disease. *Drugs* 75(15): 1797-1806, 2015
10. Pampaloni F, Reynaud EG, Stelzer EH: The third dimension bridges the gap between cell culture and live tissue. *Nat Rev Mol Cell Biol* 8(10): 839-845, 2007
11. Debnath J, Brugge JS: Modelling glandular epithelial cancers in three-dimensional cultures. *Nat Rev Cancer* 5(9): 675-688, 2005
12. Carlotti F, Bazuine M, Kekalainen T, Seppen J, Pognonec P, Maassen JA, Hoeben RC: Lentiviral vectors efficiently transduce quiescent mature 3T3-L1 adipocytes. *Mol Ther* 9(2): 209-217, 2004
13. Tsai SQ, Wyvekens N, Khayter C, Foden JA, Thapar V, Reyon D, Goodwin MJ, Aryee MJ, Joung JK: Dimeric CRISPR RNA-guided FokI nucleases for highly specific genome editing. *Nat Biotechnol* 32(6): 569-576, 2014
14. Di Z, Klop MJ, Rogkoti VM, Le Devedec SE, van de Water B, Verbeek FJ, Price LS, Meerman JH: Ultra high content image analysis and phenotype profiling of 3D cultured micro-tissues. *PLoS One* 9(10): e109688, 2014
15. Booij TH, Klop MJ, Yan K, Szantai-Kis C, Szokol B, Orfi L, van de Water B, Keri G, Price LS: Development of a 3D Tissue Culture-Based High-Content Screening Platform That Uses Phenotypic Profiling to Discriminate Selective Inhibitors of Receptor Tyrosine Kinases. *J Biomol Screen*, 2016
16. Bliss CI: The toxicity of poisons applied jointly. *Ann Appl Biol* 26(3): 585-615, 1939
17. Iversen PW, Beck B, Chen YF, Dere W, Devanarayan V, Eastwood BJ, Farmen MW, Iturria SJ, Montrose C, Moore RA, Weidner JR, Sittampalam GS: HTS Assay Validation. In: edited by Bethesda (MD), Eli Lilly & Company and the National Center for Advancing Translational Sciences, 2012,
18. Meijer L, Borgne A, Mulner O, Chong JP, Blow JJ, Inagaki N, Inagaki M, Delcros JG, Moulinoux JP: Biochemical and cellular effects of roscovitine, a potent and selective inhibitor of the cyclin-dependent kinases cdc2, cdk2 and cdk5. *Eur J Biochem* 243(1-2): 527-536, 1997

19. Maira SM, Stauffer F, Brueggen J, Furet P, Schnell C, Fritsch C, Brachmann S, Chene P, De Pover A, Schoemaker K, Fabbro D, Gabriel D, Simonen M, Murphy L, Finan P, Sellers W, Garcia-Echeverria C: Identification and characterization of NVP-BEZ235, a new orally available dual phosphatidylinositol 3-kinase/mammalian target of rapamycin inhibitor with potent in vivo antitumor activity. *Mol Cancer Ther* 7(7): 1851-1863, 2008
20. Toledo LI, Murga M, Zur R, Soria R, Rodriguez A, Martinez S, Oyarzabal J, Pastor J, Bischoff JR, Fernandez-Capetillo O: A cell-based screen identifies ATR inhibitors with synthetic lethal properties for cancer-associated mutations. *Nat Struct Mol Biol* 18(6): 721-727, 2011
21. Wilhelm SM, Carter C, Tang L, Wilkie D, McNabola A, Rong H, Chen C, Zhang X, Vincent P, McHugh M, Cao Y, Shujath J, Gawlak S, Eveleigh D, Rowley B, Liu L, Adnane L, Lynch M, Auclair D, Taylor I, Gedrich R, Voznesensky A, Riedl B, Post LE, Bollag G, Trail PA: BAY 43-9006 exhibits broad spectrum oral antitumor activity and targets the RAF/MEK/ERK pathway and receptor tyrosine kinases involved in tumor progression and angiogenesis. *Cancer Res* 64(19): 7099-7109, 2004
22. Ren XS, Sato Y, Harada K, Sasaki M, Furubo S, Song JY, Nakanuma Y: Activation of the PI3K/mTOR pathway is involved in cystic proliferation of cholangiocytes of the PCK rat. *PLoS One* 9(1): e87660, 2014
23. Santoso NG, Cebotaru L, Guggino WB: Polycystin-1, 2, and STIM1 interact with IP(3)R to modulate ER Ca release through the PI3K/Akt pathway. *Cell Physiol Biochem* 27(6): 715-726, 2011
24. Franco I, Margaria JP, De Santis MC, Ranghino A, Monteyne D, Chiaravalli M, Pema M, Campa CC, Ratto E, Gulluni F, Perez-Morga D, Somlo S, Merlo GR, Boletta A, Hirsch E: Phosphoinositide 3-Kinase-C2alpha Regulates Polycystin-2 Ciliary Entry and Protects against Kidney Cyst Formation. *J Am Soc Nephrol* 27(4): 1135-1144, 2016
25. Kampa-Schittenhelm KM, Heinrich MC, Akmut F, Rasp KH, Illing B, Dohner H, Dohner K, Schittenhelm MM: Cell cycle-dependent activity of the novel dual PI3K-MTORC1/2 inhibitor NVP-BGT226 in acute leukemia. *Mol Cancer* 12 46, 2013
26. Liu Q, Chang JW, Wang J, Kang SA, Thoreen CC, Markhard A, Hur W, Zhang J, Sim T, Sabatini DM, Gray NS: Discovery of 1-(4-(4-propionylpiperazin-1-yl)-3-(trifluoromethyl)phenyl)-9-(quinolin-3-yl)benz o[h][1,6]naphthyridin-2(1H)-one as a highly potent, selective mammalian target of rapamycin (mTOR) inhibitor for the treatment of cancer. *J Med Chem* 53(19): 7146-7155, 2010
27. Thoreen CC, Kang SA, Chang JW, Liu Q, Zhang J, Gao Y, Reichling LJ, Sim T, Sabatini DM, Gray NS: An ATP-competitive mammalian target of rapamycin inhibitor reveals rapamycin-resistant functions of mTORC1. *J Biol Chem* 284(12): 8023-8032, 2009
28. Burger MT, Pecchi S, Wagman A, Ni ZJ, Knapp M, Hendrickson T, Atallah G, Pfister K, Zhang Y, Bartulis S, Frazier K, Ng S, Smith A, Verhagen J, Haznedar J, Huh K, Iwanowicz E, Xin X, Menezes D, Merritt H, Lee I, Wiesmann M, Kaufman S, Crawford K, Chin M, Bussiere D, Shoemaker K, Zaror I, Maira SM, Voliva CF: Identification of NVP-BKM120 as a Potent, Selective, Orally Bioavailable Class I PI3 Kinase Inhibitor for Treating Cancer. *ACS Med Chem Lett* 2(10): 774-779, 2011

29. Anderson JL, Park A, Akiyama R, Tap WD, Denny CT, Federman N: Evaluation of In Vitro Activity of the Class I PI3K Inhibitor Buparlisib (BKM120) in Pediatric Bone and Soft Tissue Sarcomas. *PLoS One* 10(9): e0133610, 2015
30. Novalic Z, van der Wal AM, Leonhard WN, Koehl G, Breuning MH, Geissler EK, de Heer E, Peters DJ: Dose-dependent effects of sirolimus on mTOR signaling and polycystic kidney disease. *J Am Soc Nephrol* 23(5): 842-853, 2012
31. Shillingford JM, Murcia NS, Larson CH, Low SH, Hedgepeth R, Brown N, Flask CA, Novick AC, Goldfarb DA, Kramer-Zucker A, Walz G, Piontek KB, Germino GG, Weimbs T: The mTOR pathway is regulated by polycystin-1, and its inhibition reverses renal cystogenesis in polycystic kidney disease. *Proc Natl Acad Sci U S A* 103(14): 5466-5471, 2006
32. Robert F, Barbeau M, Ethier S, Dostie J, Pelletier J: Pharmacological inhibition of DNA-PK stimulates Cas9-mediated genome editing. *Genome Med* 7 93, 2015
33. Parker E, Newby LJ, Sharpe CC, Rossetti S, Streets AJ, Harris PC, O'Hare MJ, Ong AC: Hyperproliferation of PKD1 cystic cells is induced by insulin-like growth factor-1 activation of the Ras/Raf signalling system. *Kidney Int* 72(2): 157-165, 2007
34. Mulvihill MJ, Cooke A, Rosenfeld-Franklin M, Buck E, Foreman K, Landfair D, O'Connor M, Pirritt C, Sun Y, Yao Y, Arnold LD, Gibson NW, Ji QS: Discovery of OSI-906: a selective and orally efficacious dual inhibitor of the IGF-1 receptor and insulin receptor. *Future Med Chem* 1(6): 1153-1171, 2009
35. Zhou JX, Fan LX, Li X, Calvet JP, Li X: TNFalpha signaling regulates cystic epithelial cell proliferation through Akt/mTOR and ERK/MAPK/Cdk2 mediated Id2 signaling. *PLoS One* 10(6): e0131043, 2015
36. Ma TK, McAdoo SP, Tam FW: Spleen Tyrosine Kinase: A Crucial Player and Potential Therapeutic Target in Renal Disease. *Nephron* 133(4): 261-269, 2016
37. Torres VE, Sweeney WE, Jr., Wang X, Qian Q, Harris PC, Frost P, Avner ED: EGF receptor tyrosine kinase inhibition attenuates the development of PKD in Han:SPRD rats. *Kidney Int* 64(5): 1573-1579, 2003
38. Wilson SJ, Amsler K, Hyink DP, Li X, Lu W, Zhou J, Burrow CR, Wilson PD: Inhibition of HER-2(neu/ErbB2) restores normal function and structure to polycystic kidney disease (PKD) epithelia. *Biochim Biophys Acta* 1762(7): 647-655, 2006

## SUPPLEMENTAL MATERIALS

**SUPPLEMENTAL TABLE 1** RFNs for *Pkd1* exon 15

<i>Sequence Name</i>	<i>Target site 1</i>	<i>Target site 2</i>
<i>RFNmPKD1ex15g</i>	AGCAGGATTTCAAAGTGGAC	CTTACTTTCGGACTTCAGGT

**SUPPLEMENTAL TABLE 2** Primers flanking RFN target sites

<i>Primer name</i>	<i>Primer sequence</i>
PKD1ex15F2	CACAGTAGAGGAACCCATTGTGA
PKD1ex15R2	CACACCACCCAGTTCATTAAGG

**SUPPLEMENTAL TABLE 3** Phenotypic features incorporated in the PCA

<i>Feature</i>	<i>Image Channel</i>
area (Rhodamine)	Cytoskeleton
average_length_of_branches (Rhodamine)	Cytoskeleton
avg_wall_to_outline_center_dist (Rhodamine)	Cytoskeleton
equivdiameter (Rhodamine)	Cytoskeleton
feret (Rhodamine)	Cytoskeleton
major_Axis (Rhodamine)	Cytoskeleton
maximum_length_of_branches (Rhodamine)	Cytoskeleton
minFeret (Rhodamine)	Cytoskeleton
minor_Axis (Rhodamine)	Cytoskeleton
nNumber_of_connection_points (Rhodamine)	Cytoskeleton
number_of_branches (Rhodamine)	Cytoskeleton
number_of_end_points (Rhodamine)	Cytoskeleton
perimeter (Rhodamine)	Cytoskeleton
ratio_Area_BoundingBox_Area (Rhodamine)	Cytoskeleton
wall_count (Rhodamine)	Cytoskeleton
zernike_order_0_0 (Rhodamine)	Cytoskeleton
zernike_order_1_1 (Rhodamine)	Cytoskeleton
zernike_order_2_0 (Rhodamine)	Cytoskeleton
zernike_order_2_2 (Rhodamine)	Cytoskeleton
zernike_order_3_3 (Rhodamine)	Cytoskeleton
zernike_order_4_2 (Rhodamine)	Cytoskeleton
zernike_order_5_1 (Rhodamine)	Cytoskeleton
zernike_order_5_3 (Rhodamine)	Cytoskeleton
zernike_order_5_5 (Rhodamine)	Cytoskeleton
zernike_order_6_0 (Rhodamine)	Cytoskeleton
zernike_order_6_2 (Rhodamine)	Cytoskeleton
zernike_order_6_4 (Rhodamine)	Cytoskeleton
zernike_order_6_6 (Rhodamine)	Cytoskeleton
zernike_order_7_1 (Rhodamine)	Cytoskeleton
zernike_order_7_7 (Rhodamine)	Cytoskeleton
zernike_order_8_0 (Rhodamine)	Cytoskeleton
zernike_order_8_2 (Rhodamine)	Cytoskeleton
zernike_order_8_4 (Rhodamine)	Cytoskeleton
zernike_order_8_6 (Rhodamine)	Cytoskeleton
zernike_order_8_8 (Rhodamine)	Cytoskeleton
zernike_order_9_1 (Rhodamine)	Cytoskeleton
zernike_order_9_7 (Rhodamine)	Cytoskeleton
zernike_order_9_9 (Rhodamine)	Cytoskeleton
avg_child_to_par_center_dist (Hoechst)	Nucleus
axis_Ratio_Minor_Major (Hoechst)	Nucleus
child_count (Hoechst)	Nucleus
eccentricity (Hoechst)	Nucleus
hu_order_1 (Hoechst)	Nucleus
roundness (Hoechst)	Nucleus
zernike_order_2_2 (Hoechst)	Nucleus
zernike_order_9_3 (Hoechst)	Nucleus
zernike_order_9_5 (Hoechst)	Nucleus

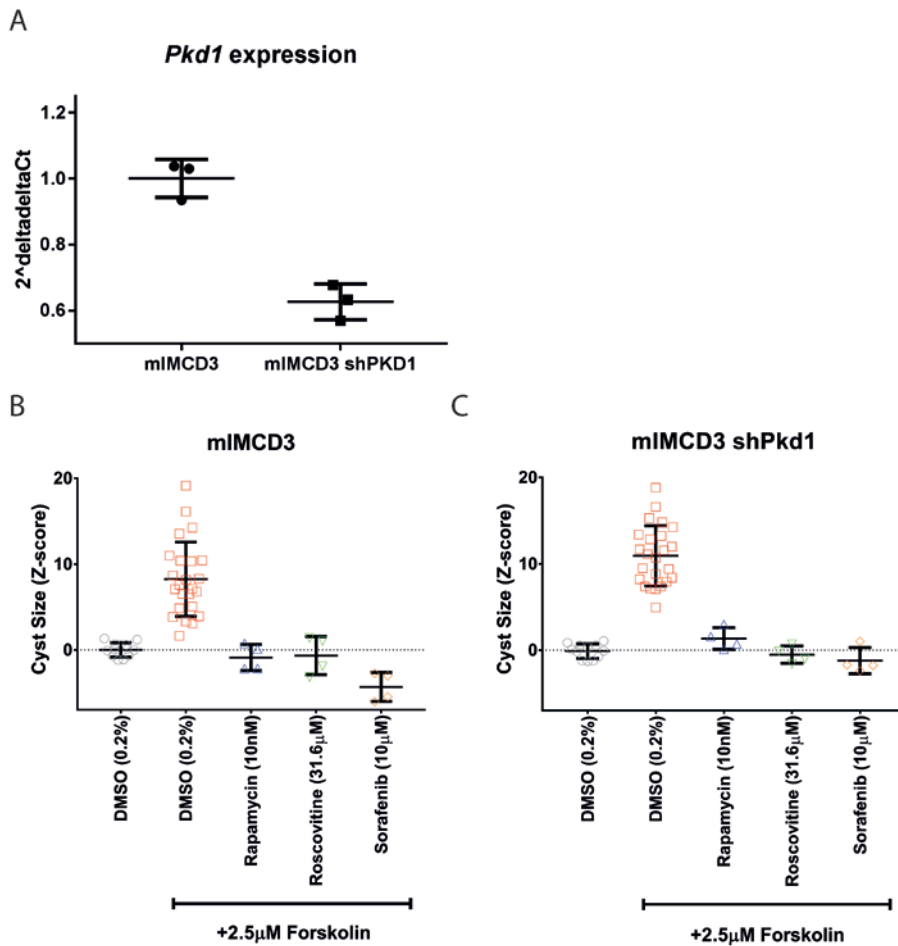
**SUPPLEMENTAL TABLE 4 Validation screen molecule information**

MOLECULES	TARGET INFORMATION	BRIEF DESCRIPTION (INFORMATION DERIVED FROM WWW.SELLECKCHEM.COM)
AG-1024 ARQ 197 (TIVANTINIB) ARRY-380 AT7867	IGF1R, IR c-Met HER2, EGFR AKT, P70 S6 kinase	Inhibitor of IGF1R/IR autophosphorylation with 7 $\mu$ M and 57 $\mu$ M, respectively. non-ATP competitive c-Met inhibitor with Ki 0.355 $\mu$ M Inhibitor of HER2 (IC50 8nM) and EGFR (IC50 4 $\mu$ M) IC50 in cell free assays: Akt2 (17nM), PKA (20nM) Akt1 (32nM), Akt3 (47nM), p70 S6K (85nM), RSK1 (>100nM)
AZD7762	CHK1, CHK2	IC50 in cell free assays: Chk1 (5nM), Chk2 (<10nM). Less potent against CAM, Yes, Fyn, Lyn, Hck and Lck.
BI 2536	PLK1	IC50 in cell free assays: PLK1 (0.83nM), PLK2 (3.5nM), PLK3 (9nM). Molecule also targets PI3K and Met >2 $\mu$ M.
BI6727 (VOLASERTIB) BUPARLISIB (NVP-BKM120) CCT137690	PLK1 PI3K (p110 $\alpha/\beta/\delta/\gamma$ ) Aurora A, Aurora B, Aurora C	IC50 in cell free assays: PLK1 (0.87nM) IC50 in cell free assays: p110 $\alpha$ (52nM) p110 $\beta$ (166nM) p110 $\delta$ (116nM) p110 $\gamma$ (262nM) IC50: Aurora A (15nM), Aurora C (19nM), Aurora B (25nM)
CHIR-124	CHK1	IC50 in cell free assays: Chk1 (0.3nM), FLT3 (5.8nM), PDGFR (6.6nM), GSK-3 (23.3nM), Fyn (98.8nM). Also targets PKA, PKC $\gamma$ , LCK, CDK2, VEGFR1, Cdc2, VEGFR2, PKC $\beta$ , PKC $\alpha$ , Chk2 <1 $\mu$ M. Kd in CHO cells: PDGFR $\alpha$ (2.1nM), PDGFR $\beta$ (3.2nM)
CRENOLANIB (CP-868596) DINACICLIB (SCH727965) EVEROLIMUS (RAD001) GSK1904529A	PDGFR- $\alpha$ , PDGFR $\beta$ CDK2, CDK5, CDK1, CDK9 mTOR IGF1R, IR	IC50 in cell free assays: CDK2 (1nM), CDK5 (1nM), CDK1 (3nM), CDK9 (4nM). Also blocks thymidine DNA incorporation. IC50 in cell free assays: mTOR (FKBP12) (1.6-2.4nM) IC50 in cell free assays: IR (25nM), IGF1R (27nM), B-Raf (>2 $\mu$ M) and others at higher concentrations.
GSK461364 HESPERADIN HMN-214	PLK1 Aurora B PLK1	Ki in cell free assay: PLK1 (2.2nM) IC50 in cell free assays TBAUK1 (40nM), Aurora B (250nM) Prodrug of HMN-176. Little in vitro data is available but causes cytotoxic effects in nM-range.
IMD 0354 KX2-391 LDN193189	IKK- $\beta$ Src ALK2, ALK3	Affects NF $\kappa$ B nuclear translocation >0.5 $\mu$ M. Growth inhibition in cancer cell lines GI 9-60nM. Inhibits transcriptional activity of ALK2 (5nM) and ALK3 (30nM) receptors in cell-based assays.
LINSITINIB (OSI-906) LY2603618 (IC-83) MUBRITINIB (TAK 165) NU7441 (KU-57788) NVP-ADW742 ON-01910 OSU-03012 PD 0332991 (PALBOCIC LIB) HCL PDI73074 PIK-75	IGF1R, IR CHK1 HER2 DNA-PK IGF1R PLK1 PDK-1 CDK4, CDK6 FGFR1, VEGFR2 DNA-PK, PI3K (p110 $\alpha$ , $\beta$ , $\gamma$ and $\delta$ )	Inhibits IR (75nM) and IGR1R (35nM) in cell-free assays. Inhibits CHK1 (IC50 7nM) in vitro. HER2 inhibitor with IC50 of 6nM in BT-474 cells. Inhibits DNA-PK with IC50 14nM, mTOR at 1.7 $\mu$ M and PI3K at 5 $\mu$ M Inhibits IGF1R with IC50 170nM Inhibits PLK1 with IC50 9nM in cell-free assays. IC50 5 $\mu$ M, derivative of celecoxib. IC50 in cell free assays: CDK4/CyclinD3 (9nM), CDK4/CyclinD1 (11nM), CDK6/CyclinD2 (15nM) IC50 in cell free assays: FGFR1 (25nM), VEGFR2 (100-200nM), c-Src (19.8 $\mu$ M) IC50 in cell free assays: DNA-PK (2nM), p110 $\alpha$ (5.8nM), p110 $\beta$ (1.3 $\mu$ M), p110 $\gamma$ (76nM), p110 $\delta$ (0.51 $\mu$ M)
PIK-90	PI3K (p110 $\alpha$ , $\beta$ , $\gamma$ and $\delta$ )	IC50 in cell free assays: p110 $\alpha$ (11nM), p110 $\beta$ (350nM), p110 $\gamma$ (18nM), p110 $\delta$ (58nM)
QUIZARTINIB (AC220) R406 R406(FREE BASE) R788 (FOSTAMATINIB) R935788 (FOSTAMATINIB DISODIUM, R788 DISODIUM) THIAZOVIVIN TORIN-1	FLT3 Syk Syk Syk Syk ROCK mTOR (mTORC1/2)	IC50 in cell lines: FLT3 (IDT) (1.1nM), FLT3 (WT) (4.2nM). Kd for FLT3 1.6nM. Inhibits Syk with IC50 41nM in cell free assays. Also inhibits FLT3. Inhibits Syk with IC50 41nM in cell free assays. Also inhibits FLT3. Prodrug of R406, Syk inhibitor with IC50 of 41nM Prodrug of R406, Syk inhibitor with IC50 of 41nM Inhibits ROCK in low micromolar range. IC50 of 2nM/10nM for mTORC1/2, respectively. 1000-fold selectivity for mTOR over PI3K.
TPCA-1	IKK- $\beta$ , IKK- $\alpha$	In a cell free assay, TPCA-1 inhibits IKK- $\beta$ with an IC50 of 17.9nM, IC50 against IKK- $\alpha$ 400nM, and JNK3 3600nM.
TWS119 TYRPHOSTIN AG 879 (AG 879) VANDETANIB (ZACTIMA) WP1130	GSK-3 $\beta$ HER2 VEGFR, EGFR Deubiquitinase (USP5, UCH-L1, USP9x, USP14, and UCH37) and Bcr/Abl, JAK2, STAT	IC50 in cell free assays: GSK-3 $\beta$ (30nM) Inhibits HER2 with an IC50 of 1.0 $\mu$ M Inhibits VEGFR2 in cell free assays with an IC50 of 40nM. Also inhibits VEGFR3 and EGFR with IC50 110nM and 500nM. Degrasyn is a deubiquitinase that also inhibits Bcr/Abl at 1.8 $\mu$ M
WYE-125132 WZ3146	mTOR EGFR	Potent mTOR inhibitor with an IC50 of 0.19nM. Highly selective over PI3Ks. Mutant-selective EGFR inhibitor with IC50 2-14nM. <100-fold less potent against WT EGFR.
WZ8040 ZSTK474	EGFR PI3K (p110 $\alpha$ , $\beta$ , $\gamma$ and $\delta$ )	Mutant-selective irreversible EGFR inhibitor. <100 fold less potent against WT EGFR IC50 in cell free assays: p110 $\alpha$ (16nM), p110 $\beta$ (44nM), p110 $\gamma$ (49nM), p110 $\delta$ (4.6nM)

**SUPPLEMENTAL TABLE 5** Statistical significance of selected hits

COMPOUND	Conc. ( $\mu$ M)	ONE WAY ANOVA WITH DUNNETT'S MULTIPLE COMPARISON TEST (P<0.05)*		Correlates
		Primary Screen	Validation Screen	
AG-1024	1	0.9995	0.9915	Yes
ARQ 197	1	0.0004	0.0001	Yes
ARRY-380	1	0.999	0.9991	Yes
AT7867	0.1	0.1666	0.9913	Yes
AZD7762	0.1	0.0004	0.9996	No
BI 2536	0.1	0.0001	0.0001	Yes
BI6727	0.1	0.0458	0.9803	No
CCT137690	0.1	0.0001	0.9986	No
CHIR-124	0.1	0.0001	0.0001	Yes
CRENOLANIB	1	0.0008	0.0686	No
DINACICLIB	0.1	0.0001	0.0001	Yes
EVEROLIMUS	0.1	0.0001	0.0001	Yes
GSK1904529A	1	0.4917	0.0147	No
GSK461364	0.1	0.0058	0.898	No
HESPERADIN	1	0.0001	0.0001	Yes
HMN-214	0.1	0.0001	0.9995	No
IMD 0354	1	0.0001	0.0001	Yes
KX2-391	0.1	0.0057	0.0001	Yes
LDN193189	1	0.0001	0.9991	No
LINSITINIB	1	0.0001	0.0001	Yes
LY2603618	0.1	0.0011	0.9991	No
MUBRITINIB	0.1	0.024	0.0007	Yes
NU7441	0.1	0.0002	0.9835	No
NVP-ADW742	0.1	0.0001	0.9985	No
ON-01910	1	0.0001	0.0001	Yes
OSU-03012	1	0.0001	0.9997	No
PD 0332991	1	0.0001	0.0145	Yes
PD173074	1	0.9995	0.87	Yes
PIK-75	1	0.0001	0.0001	Yes
PIK-90	1	0.1057	0.1812	Yes
QUIZARTINIB	1	0.0186	0.0086	Yes
R406	1	0.0067	0.0125	Yes
R406 (FREE BASE)	0.1	0.0001	0.3736	No
R788	1	0.0193	0.0001	Yes
R935788	1	0.3575	0.0001	No
THIAZOVIVIN	1	0.603	0.9994	Yes
TPCA-1	1	0.0002	0.8242	No
TWS119	1	0.9808	0.9996	Yes
TYRPHOSTIN	1	0.9981	0.007	No
AG 879	1	0.9981	0.007	No
VANDETANIB	1	0.1431	0.3565	Yes
WP1130	1	0.0001	0.0943	Yes
WYE-125132	0.1	0.0001	0.0001	Yes
WZ3146	0.1	0.0001	0.592	No
WZ8040	0.1	0.0001	0.6997	No
ZSTK474	1	0.0001	0.4663	No

\*Statistical significance was assessed compared to forskolin-stimulated controls using ordinary one-way ANOVA with Dunnett's multiple comparison test. Differences were considered significantly different for adjusted P<0.05.



**SUPPLEMENTAL FIGURE 1** *Pkd1* expression is reduced in mIMCD3 shPkd1 cells. **A**) qPCR showing reduced expression of *Pkd1* using the  $z^{\Delta\Delta Ct}$  method (means  $\pm$  SD of triplicates). qPCR was performed three times. **B** and **C**) Control conditions in both mIMCD3 wt and mIMCD3 shPkd1 cells. Cyst growth depicted by cyst size z-scored to unstimulated control (DMSO 0.2%, grey circles) median (dotted black line at  $y=0$ ). Induction of cyst growth by forskolin demonstrated by red squares. Individual datapoints and mean  $\pm$  SD shown.

**A**

## miMCD3 clone 5E4

```
Gtcaagatcaagctgagaaccagtgggtcagctcaatgccacagttgaagtggccataca
gggtcctctgggtggcctgagatcagaaccagttagccaagatagcatcttctggcagctg
gtcccactotacocctctctgggtcagctgctgaaggtaccaatgtgacttggctggaac
ttgcaggtggagtaaggaacgacagctacatctgctgctgctctccacgctggcagttt
ctctctgcaactcaatgcttccaatgcaatcagttgggtctcagccaatgtacaacctacag
tagaggaacccctgtgaaacccgataccttgggccaagcagcaagggtggccctggcag
ccagtcacccttggaaacccctgctggcaactggctctgctcttaacttccgaccccaagctgg
gggtctctccctgaaagtgtccctagcccccaactctcccaacag
```

Clone 5E4 primerset 1 (wt: 124bp, ko: 99bp)  
 F: CCATTGTGAACCTGATGCTG  
 R: ACAGACCCACCAACTGAAG

Clone 5E4 primerset 2 (wt: 128bp, ko: no band)  
 F: TGCAGTCAGTTGGGTCTCAG  
 R: CTGCCAGCAGGATTTCAAAG

**B**

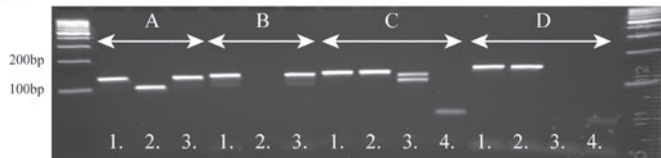
## miMCD3 clone 31

```
cgtatggctcaaatggtactgctggtgtggatgtgagccgaccccaagctgggtgccacggctggcaactcct
gtggccaactactcttgggttgggtttcatttgggacacacacattggcacggagcatocagcccaatgtg
acagtggctgctccctctctgggtaccctcaatgaaggtgctcataccgggatagttcaacacgcaagctg
gtgctggatgggacaaagctctatgacctaattagagatggtagatgcaacgctcaacttccatgggctc
tgcgtgcttcaacacagatgagacaggtggctgctgctgctaaacttgggcccctggg
```

Clone 31 primerset 1 (wt: 133bp, ko:123bp)  
 F: GAGCGTCTGGTACCCATCAT  
 R: AATGGAAGTTGAGCGGTGTC

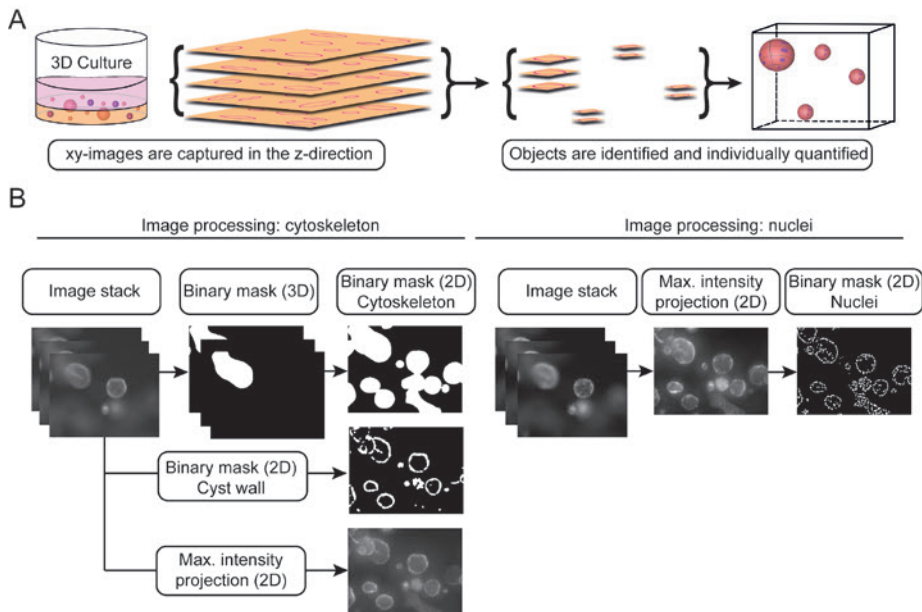
Clone 31 primerset 2 (wt: 145bp, ko: no band)  
 F: GGGCCACTACTGCTTTGTGT  
 R: GTCCTGCGTGTCTGACCATA

Start of exon 16

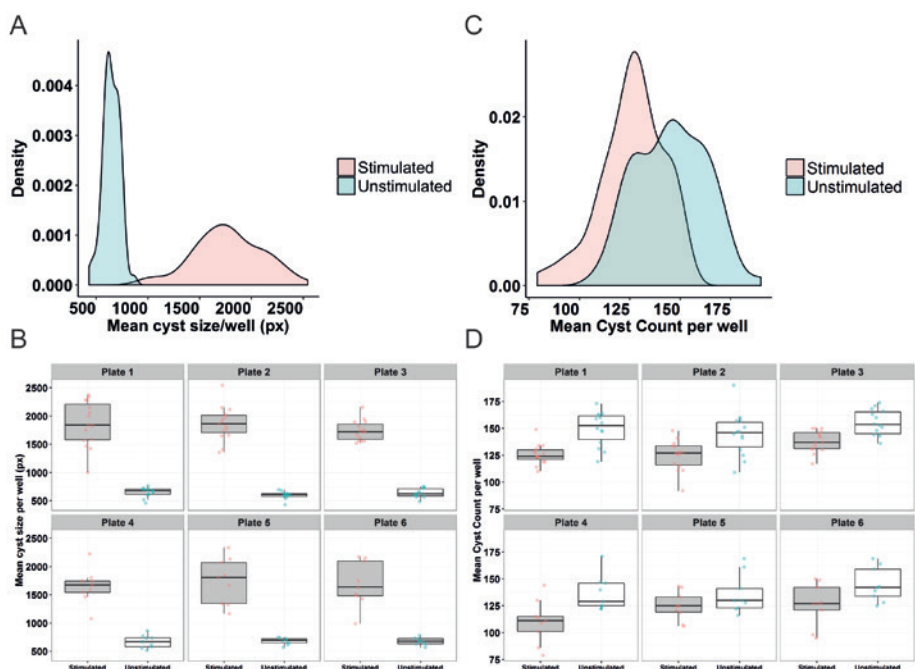
**C**

- |                     |                          |
|---------------------|--------------------------|
| 1. miMCD3 wt        | A. Clone 5E4 primerset 1 |
| 2. miMCD3 clone 5E4 | B. Clone 5E4 primerset 2 |
| 3. miMCD3 clone 31  | C. Clone 31 primerset 1  |
| 4. -RT              | D. Clone 31 primerset 2  |

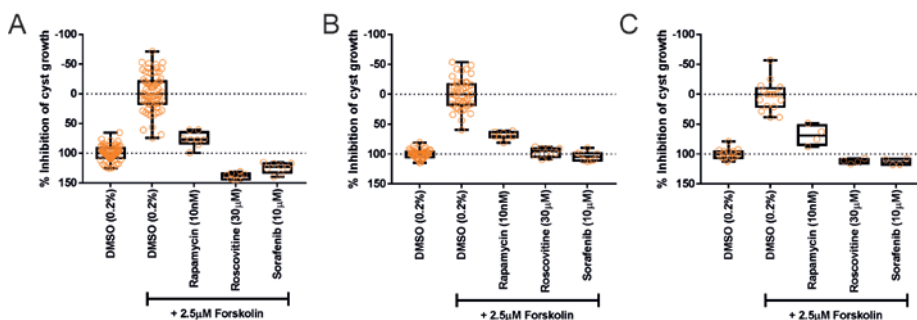
**SUPPLEMENTAL FIGURE 2** Generation of *Pkd1* knockout cell lines. **A** and **B**) primer sets for both 5E4 and 31 clones for PCR depicted in C. **C**) PCR revealing deletion in *Pkd1* gene in clone 5E4 and clone 31. Clone 5E4 was selected due to improved growth characteristics.



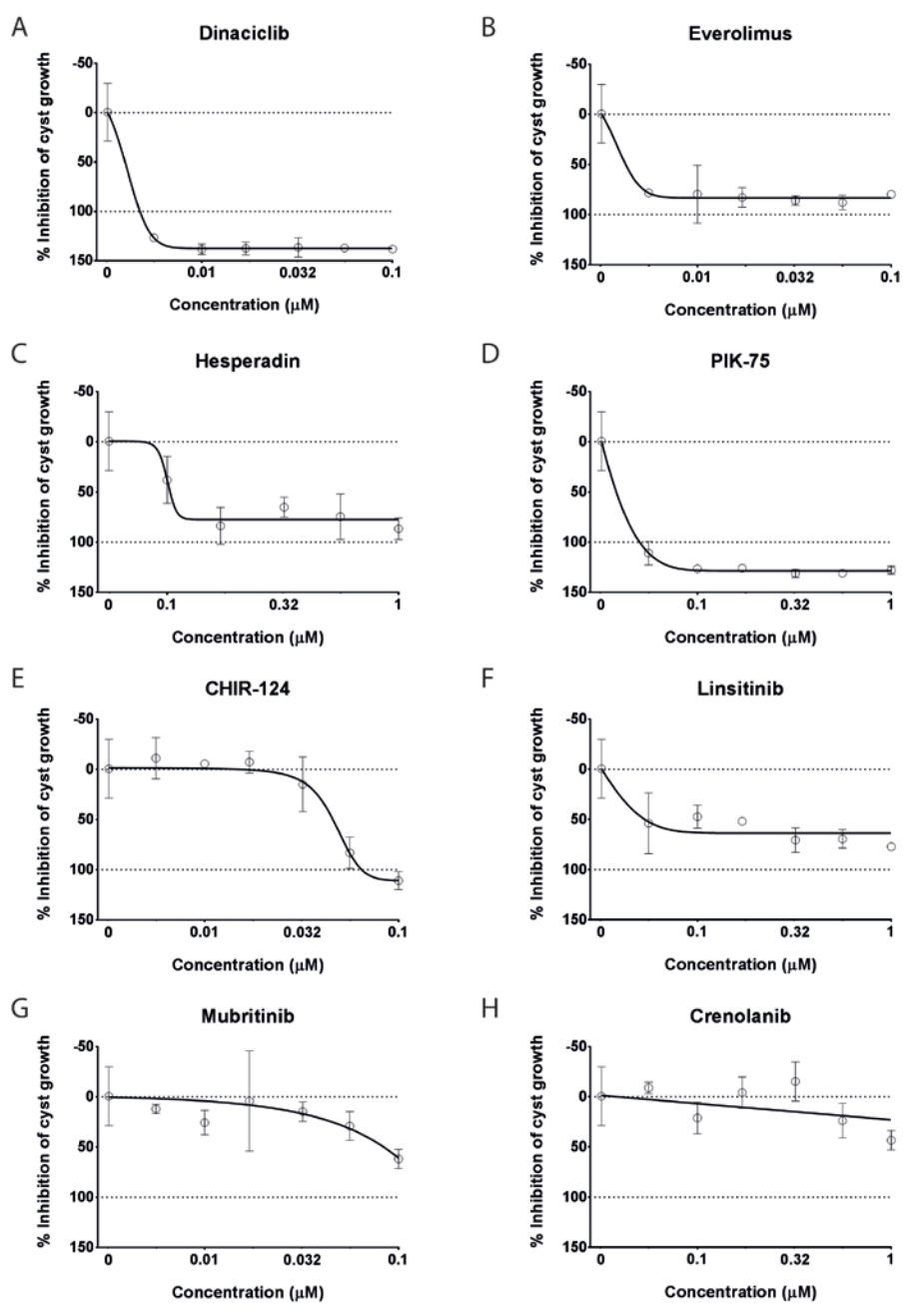
**SUPPLEMENTAL FIGURE 3** Schematic representation of image analysis procedure. **A)** Images are captured at  $50\mu\text{m}$  intervals throughout the z-axis of the gel and objects are extracted from each image plane and individually quantified. **B)** Image stacks (cutouts shown) of approximately 25 images per well from both cytoskeleton and nucleus image channels are processed to binary masks for quantification of phenotypic descriptors.



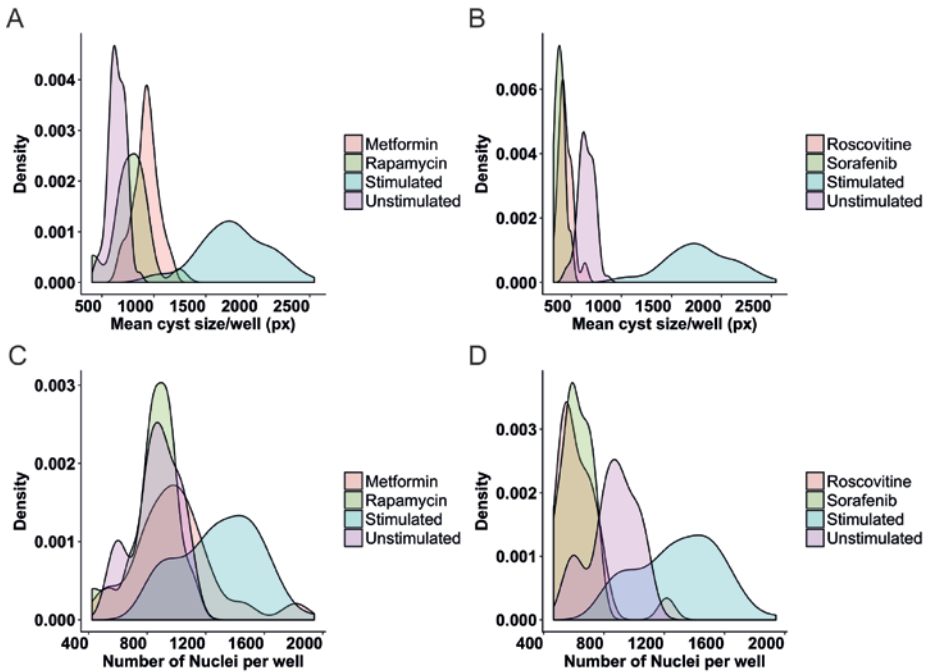
**SUPPLEMENTAL FIGURE 4** Forskolin-treatment increases cyst growth. **A)** Density plot of validation screen showing non-normalized cyst size from all six plates in the validation for unstimulated (0.2% DMSO) and stimulated (2.5 $\mu$ M forskolin) conditions. **B)** Increased cyst growth after forskolin treatment is highly similar over different plates. **C)** As in A, but showing the number of cysts per well. **D)** As in B, number of cysts per well is similar among the six plates.



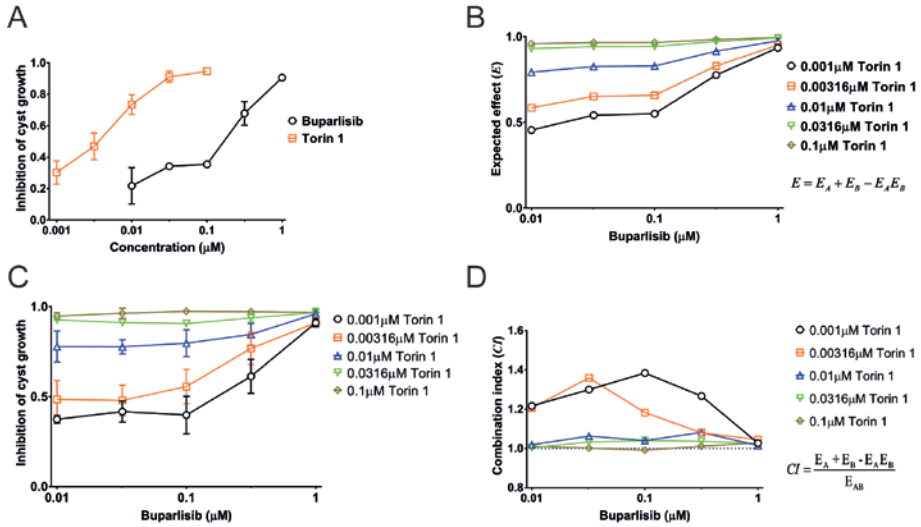
**SUPPLEMENTAL FIGURE 5** Forskolin-induced mIMRFNPKD 5E<sub>4</sub> cyst growth is inhibited by rapamycin, roscovitine and sorafenib in three independent experiments (A,B,C). Individual wells shown as orange circles. Box plot whiskers represent min to max.



**SUPPLEMENTAL FIGURE 6** Concentration- cyst growth inhibition curves of data presented in main figure 4A. Black circles represent mean values of three wells (technical replicates) and error bars represent SD to illustrate intra-experimental variation. In case when error bars are not visible, the SD is smaller than the symbol height. **A)** Dinaciclib, **B)** Everolimus, **C)** Hesperadin, **D)** PIK-75, **E)** CHIR-124, **F)** Linsitinib, **G)** Mubritinib, **H)** Crenolanib.



**SUPPLEMENTAL FIGURE 7** Roscovitine and sorafenib may affect cyst phenotype by reducing cell number. This data is derived from the validation screen as depicted in figure 4 and supplemental figure 4. **A)** Density plot as in supplemental figure 4 showing that 5mM metformin and 10nM rapamycin (pink and yellow) slow forskolin-induced cyst growth compared to stimulated (2.5 $\mu$ M forskolin, blue) condition. **B)** Roscovitine (31.6 $\mu$ M, pink) and sorafenib (10 $\mu$ M, yellow) slow forskolin-induced cyst growth compared to stimulated (2.5 $\mu$ M forskolin, blue) condition. **C)** Metformin and rapamycin do not cause a reduction in the number of nuclei (as derived from a maximum intensity projection of a 3D image stack) relative to unstimulated (0.2% DMSO vehicle, purple) control. **D)** Roscovitine (pink) and sorafenib (yellow) lower the number of nuclei (as derived from a maximum intensity projection of a 3D image stack) relative to the unstimulated condition (0.2% DMSO vehicle, purple).



**SUPPLEMENTAL FIGURE 8** Assessment of synergistic effects of mTOR inhibitor torin 1 and PI3K inhibitor buparlisib (NVP-BKM-120) in mIMRFNPKD 5E4 cells. When combined, these inhibitors do not cause synergistic potentiation of cyst growth inhibition. **A**) Experimental measurement of inhibition of forskolin-induced cyst growth by buparlisib and torin 1 scaled between 0 (no inhibition) and 1 (max inhibition). Data presented represent means  $\pm$  SD of four wells (technical replicates). In case when error bars are not visible, the SD is smaller than the symbol height. **B**) Predicted inhibitory activity of combinations of torin 1 and buparlisib, scaled between 0 (no inhibition) and 1 (max inhibition). This prediction used the formula  $E = E_A + E_B - E_A E_B$  where  $E_A$  is the effect of torin 1 and  $E_B$  is the effect of buparlisib **C**) Experimental measurement cyst growth inhibition by combinations of buparlisib and torin 1. Response scaled between 0 (no inhibition) and 1 (max inhibition). Data presented represent means  $\pm$  SD of four wells (technical replicates). In case when error bars are not visible, the SD is smaller than the symbol height. **D**) Combination index  $CI$  was defined by dividing the predicted response  $E$  with the observed response of combinatory therapy  $E_{AB}$ . A  $CI < 1$  indicates synergistic effects, a  $CI > 1$  indicates antagonistic effects, in contrast to an expected additive effect when  $CI = 1$ . The observed effect of some conditions (e.g. 0.00316 $\mu\text{M}$  torin 1 and 0.1 $\mu\text{M}$  buparlisib) in C was mildly less potent than the effects predicted in B, causing  $CI > 1$ . For other combinations,  $CI$  was 1, indicating only additive effects.

